LUNFD6/(NFFL-7126) 1996
October 5, 1996

Detecting B_c mesons in the ATLAS experiment at LHC

Diploma work

Magnus Peterson [1]
Department of Physics
Lund University, Box 118
S-221 00 Lund, Sweden

Abstract

The possibility of observing the signal from B_c mesons in the ATLAS experiment at the Large Hadron Collider was studied. The decay mode studied was $B_c \to J/\psi\pi$ followed by the leptonic decay $J/\psi \to e^+e^-$. An estimate of the number of produced B_c per year was done combined with a study of the background. The resolution of the B_c-mass was determined.

[1] Magnus.Peterson@quark.lu.se

Contents

1 Introduction **3**

2 Physics **4**

2.1 Basics of Particle Physics 4

2.2 The physics of a particle accelerator 6

2.3 Kinematical variables 7

3 CERN, LHC and the ATLAS detector **11**

3.1 CERN 11

3.2 The LHC accelerator 12

3.3 The ATLAS detector 14

3.3.1 The Inner detector 14

3.3.2 Calorimeters and muon system 17

3.4 The field of B-physics at ATLAS 19

4 How to find the B_c **21**

4.1 Properties of the decay 21

4.2 The trigger for B-physics 22

4.3 Parameters of the track 23

4.3.1 A simple vertex algorithm 24

5 Simulation and reconstruction **27**

5.1 Event generation 27

5.2 The analysis program 30

6 Results **33**

6.1 Introduction 33

6.2 The B_c-signal analysis 34

6.3 The background analysis 36

6.4 Conclusions 40

6.5 Outlook 41

A The invariant mass **43**

Chapter 1

Introduction

The aim of physics is to get a better understanding of nature, to learn how and why things work as they do. To do that you create a theory of how you think it works, and hopefully test your theory to see if it make sense. In the field of particle physics, the concept of matter has been described in the so called Standard Model. The reason for doing experiments at big colliders is to study this theory.

The aim of the ATLAS experiment is with the help of the powerful collider LHC to look for more massive particles than ever found before. The "most wanted" particle is the so called Higgs boson which has the key to why particles have mass. Among the massive particles is the object of my study , the B_c meson.

In the following two chapters I will try to explain the physics involved and the experiment itself. Chapter 4 - 6 will be dedicated to the B_c meson. The results of my study are presented partly in Chapter 5 and in Chapter 6.

Chapter 2

Physics

2.1 Basics of Particle Physics

Everybody knows that the nucleus is made up by protons and neutrons. The number of protons (matching the number of electrons) decides which element the atom belongs to. Experiments have revealed that the proton and neutron

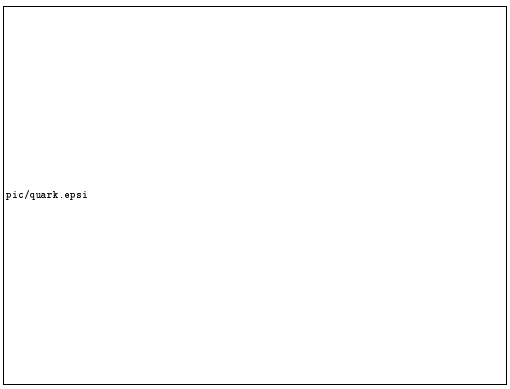

are built up by even smaller particles - the *quarks* [1]. The proton consists of two u-quarks and one d-quark while the constituents of the neutron are two d-quarks and one u-quark. To create matter we only need these quarks and the electron, that belong to the group of particles called leptons.

Still, there are other types of quarks and leptons. The model of today, *The Standard Model*, separates the existing quarks and leptons into three families:

[1] "Three quarks for Muster Mark" - in James Joyce's book Finnegans Wake

- Family 1: Contains the particles needed to explain the matter we see outside the laboratory. In this first family, we have the two lightest quarks and leptons: the u- and d-quark together with the *electron* and the $electron - neutrino$ (ν_e).

- Family 2: Contains the s- and c-quarks. The s-quark was discovered in cosmic ray experiments in the 1960s while the c-quark only can be found in accelerator experiments. This second family also contains two leptons. The *muon* which is 200 times heavier than the electron, but otherwise identical, and the $muon - neutrino$ (ν_μ).

- Family 3: The particles in the third family are the heaviest, only observable in particle accelerators. They are the b- and t-quark and the leptons *tau* and $tau - neutrino$ (ν_τ).

The leptons are thought to be pointlike with integer charge while the quarks have fractional electrical charge. All the listed leptons and quarks in tab. 2.1

Family / Charge	1	2	3
-1	e	μ	τ
0	ν_e	ν_μ	ν_τ
2/3	u	c	t
-1/3	d	s	b

Table 2.1: The three generations of particles. All these particles exist in anti-states with opposite sign in quantum numbers.

also exist in anti-particle states. They have the same mass but with opposite sign in quantum numbers. Anti-particles, besides the charged leptons and hadrons, are often denoted with a bar-sign. The quarks can build up particles in states of three quarks called baryons, for example the proton. They also combine in quark and anti-quark states called mesons. The object of my study, B_c, exists in the two charged meson states

$$B_c^+ = \bar{b}c \qquad\qquad B_c^- = \bar{c}b.$$

The quarks possess another degree of freedom called colour charge. Each quark can exist in one of the three colour charged states *red*, *green* and *blue*.

There are four interactions (forces) taking place among particles. They are the electromagnetic, strong, weak and gravitational interactions. These forces are mediated by different bosons i.e. particles with integer spin.

An electrical charged particle can emit a photon thus getting a recoil while the photon can be absorbed by another charged particle getting a thrust. The electromagnetic interaction between the particles is then understood as an exchange of photons.

The strong interaction is mediated by the gluon, carrying the colour charge. The gluons are massless particles and exist in 8 colour states. The difference between the electromagnetic and the strong force is that the gluons carry colour charge while the photon is electrically neutral, implying that the gluons can interact with each other. Another difference is that the strong force have three colour charges. The strong force is responsible for the fact that quarks only exist in bound states.

The weak interactions have the capability to transform quarks and leptons into others of their kind. This interaction is mediated by the massive W- and Z-bosons. As an example a c-quark can emit a W^+ transforming to an s-quark. The W^+ will decay into a $q_1\bar{q}_2$-pair or a lepton-pair. The process can be illustrated in a Feynman-diagram like fig. 2.1, which is a pictorial technique to illustrate an interaction. The weak interaction is among other things responsible for the radioactive decay.

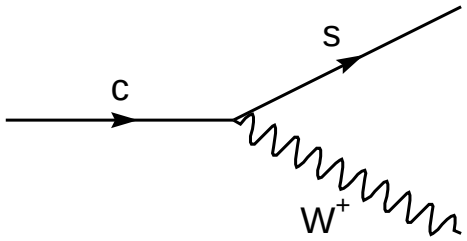

Figure 2.1: The principal of a Feynman-diagram.

2.2 The physics of a particle accelerator

To investigate the inner most structure of matter one has to work at short distances with high precision. The quantum mechanical wave nature of high energy particle probes allow us to do this. The wavelength of a probe, the distance between wave peaks, must be smaller than the objects we are trying to measure. One should also remember that in accelerated particle beams one deals with very energetic particles (relativistic) so the rest mass can be

neglected. For photons and massive particles the relation

$$\lambda = \frac{h}{p} = \frac{hc}{\sqrt{E^2 - m^2c^4}} \propto \frac{1}{E}$$

states that the wavelength is inversely proportional to the energy of the particles. Hence the smaller objects we want to study, the higher energy we need. From the fact that mass and energy are interchangeable the collision energy can be increased and in that way create more massive particles.

In the Large Hadron Collider (LHC) the idea is to collide protons with an energy of 7 TeV each, i.e. a centre of mass energy of 14 TeV in a head-on collision. With this energy it will be possible to create the massive particle B_c.

The basic tools at CERN are the accelerators. They provide high-energy particles to different experiments. The concept of an accelerator is that when a charged particle is exposed to an electric potential, the particle is accelerated. The proton, which is of positive charge, "feels" the negative potential from the plate with the hole and accelerates towards it. When the proton reaches the hole the potential is changed to zero. The acceleration has increased the protons kinetic energy[2]. By placing a lot of such plates (called RF-cavities) in a row one repeats the acceleration process. If you then place dipole-magnets which bend the trajectory of the particles forming a circle, the same acceleration-plate can be passed many times.

Quadrupole-magnets are placed in the accelerator to focus the beam to be as compact as possible. The advantage with the circular accelerator is that it does not waste as much energy as linear accelerators, where the beam interacts at one point and only once. In a storage ring (circular accelerator) the bunches collide again and again. The disadvantage with a circular collider is that when the particles are bent in a magnetic field they loose energy due to synchrotron radiation, with an energy loss $\propto (E/m)^4$. This explains why a pp-collider is built and not a e^+e^--collider. At these experiments on the circular path the *detectors* are mounted to analyse the interaction of the particles in the beam.

2.3 Kinematic variables

Relativistic calculations are simplified by the use of four vectors which contain information about energy and momenta, $\vec{P} = (\frac{E}{c}, p_x, p_y, p_z)$.

[2] If the potential is -100 V the particle gains 100 eV in kinetic energy.

Properties that remain the same in all inertial systems are called invariants. An important invariant is the invariant mass W for a system of particles. It is defined as

$$W^2c^4 = (E_1 + E_2 + \ldots + E_N)^2 - (\vec{p_1} + \vec{p_2} + \ldots \vec{p_N})^2c^2$$

for a system of N particles. In the centre of mass frame where $\sum p_i = 0$ the invariant mass is equal to the centre of mass energy. For a single particle the invariant mass is equal to the rest mass. The invariant mass of a particle system is easily understood by the concept of four-momenta. In Appendix A the invariant mass is explained by the use of four-momenta.

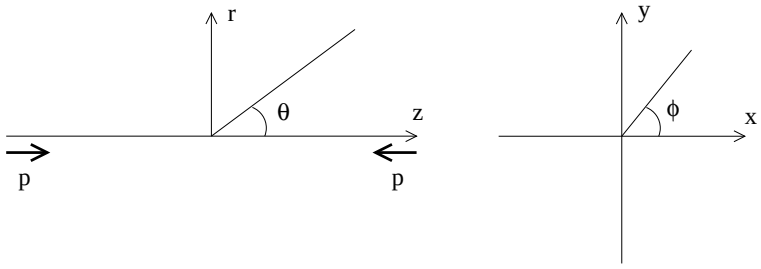

Figure 2.2: The coordinate system in the ATLAS detector. The radius r defined as $r = \sqrt{x^2 + y^2}$.

The coordinate system of the detector is important. In fig. 2.2 the beam direction is defined along the z-axis. The transverse momenta, p_{T}, plays an important rôle in the experiment. It is defined as the projection of a particles momenta to the $r\phi$-plane

$$p_{\mathrm{T}} = \sqrt{p_x^2 + p_y^2}$$

perpendicular to the beam direction.

In special relativity one often constructs an entity called rapidity, y, defined as as

$$y = \frac{1}{2} \ln \frac{E + p_z}{E - p_z} = \tanh^{-1} \frac{p_z}{E} \tag{2.1}$$

where E is the energy of the particle. Applying a Lorentz-transformation in the z-direction from a system with rapidity y to a moving system with rapidity y_1 gives us the new rapidity as $y \rightarrow y + y_1$, i.e. the rapidity is additive. In the limit of negligible rest mass the rapidity of eq. 2.1 can be expanded in a power series. If this calculation is made one gets a new variable depending only on the angle θ. It is calculated to be

$$\eta = -\ln \tan \frac{\theta}{2}$$

and is called pseudorapidity, giving a non-linear measurement of the angle. It is understood as a geometrical variable of the detector and you can define the positions of the different detectors in this sense. From the coordinate

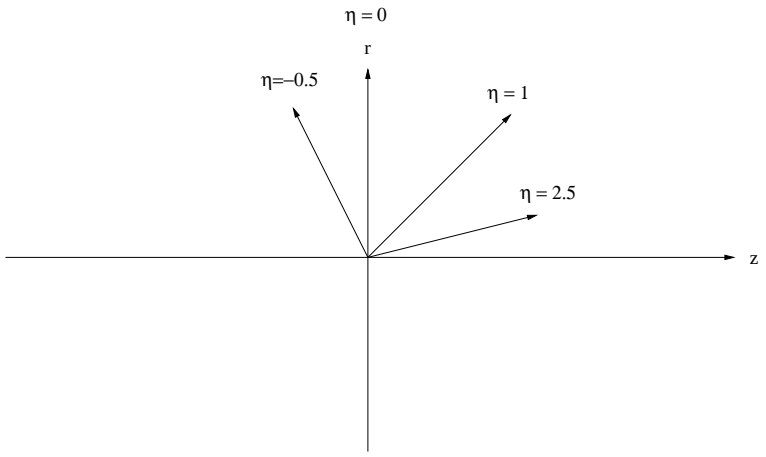

Figure 2.3: Illustration of the pseudorapidity.

system of the detector the pseudorapidity is illustrated in fig. 2.3.

Experimentally observable interaction rates depend on the laws of physics, which one cannot control, and on how frequently particles are brought together to collide, which can be controlled. In a collider, it is possible to adjust the density of particles in the two beams and the size of their crossing area. This variable is called the luminosity, $\mathcal{L}$, of the machine.

In particle physics one often uses the concept cross section. This is a measure of the relative probability for a reaction to take place. If a reaction occur at a certain rate, dN/dt, and the experiment is running at the luminosity $\mathcal{L}$ $[\mathrm{cm}^{-2}\mathrm{s}^{-1}]$, the cross section for that process is defined as

$$\sigma = \frac{\frac{dN}{dt}}{\mathcal{L}} \tag{2.2}$$

being a constant. To keep the interaction rates at experimentally observable levels, one can increase the luminosity of the machine. The luminosity is often expressed as the integrated luminosity. It is defined as

$$L = \int \mathcal{L} dt$$

integrated over the time the experiment is running. Rewriting eq. 2.2 gives us the integrated luminosity as

$$L = \int \mathcal{L} dt = \int \frac{1}{\sigma} \cdot \frac{dN}{dt} dt = \frac{1}{\sigma} \int dN = \frac{N_{tot}}{\sigma} \tag{2.3}$$

i.e. the number of produced reactions is the integrated luminosity times the cross section of the reaction. Cross sections are often expressed in units of barn, $1\mathrm{b} = 10^{-28}\mathrm{m}^2$. The integrated luminosity is usually written in units of b^{-1}.

Chapter 3

CERN, LHC and the ATLAS detector

3.1 CERN

Le Conceil Europeén pour la Recherche Nucléaire (CERN) is one of the largest research centres in the world with nineteen member states. It is placed near the city of Geneva, at the border between Switzerland and France. The laboratory is among the world leading laboratories in experimental particle physics, but also nuclear, atomic and solid state physics are represented in different experiments.

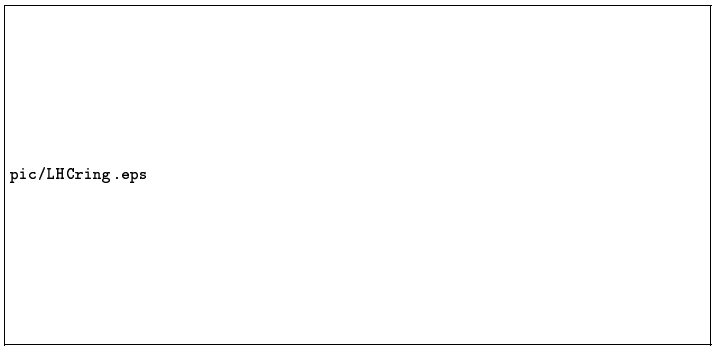

Figure 3.1: The different accelerators at CERN.

The first accelerator built at CERN was the Synchro Cyclotron (SC) capable of accelerating protons to 600 MeV. The main activity was experiments

in nuclear physics analysing short-lived isotopes.

The first accelerator specified for particle physics was the Proton Synchroton (PS) built in 1959 with ability to accelerate protons to 28 GeV, a fantastic energy in those days. Nowadays it is used for testbeams and as an injector to the larger accelerators.

In 1976 the Super Proton Synchroton (SPS) was ready. Protons are supplied from the PS with an energy of 10 GeV and injected into the 7 km long SPS-ring being accelerated up to 500 GeV before colliding at the experiments. Among the results from the SPS are the deep inelastic experiments with neutrinos and muons which confirmed the quark model. A few years later (1981) the SPS was used for a new purpose, as a storage ring with counter rotating protons and anti-protons. The purpose was to get enough energy to produce the predicted Z^0- and W-particles, which were successfully identified in 1982 in the UA1 and UA2 experiments.

The latest built accelerator (1989) at CERN is the Large Electron Positron collider (LEP). 3 304 bending magnets are placed one hundred meters below ground in a 27 km long tunnel. The machine collides electrons and positrons at sufficient energy to produce the Z^0 and in the LEP2 (summer 1996) W-particles, to get a better mass determination than the proton colliders. Many studies have been made using LEP, among the results are the determination that there exist only three different families. Four different experiments are placed at points where electrons and positrons collide.

3.2 The LHC accelerator

The Large Hadron Collider is under construction and will be built in the existing LEP-tunnel where the current accelerator LEP will be removed. If everything goes as planned the accelerator will start in 2005, colliding protons with a centre of mass energy of 14 TeV.

The protons will be delivered from the SPS and its pre-accelerators at 0.45 TeV. The reasons for not injecting the protons into LHC directly are two. The accelerators focuse the beam i.e. the proton bunches, so that the beam is so small as possible when it is injected into LHC. In this way the aperture of the magnets does not need to be so sensitive for lower fields. Another argument is that when the protons circle the ring under influence of a magnetic field they oscillate. The oscillations occur with an amplitude A as

$$A \propto \frac{1}{\sqrt{E}}$$

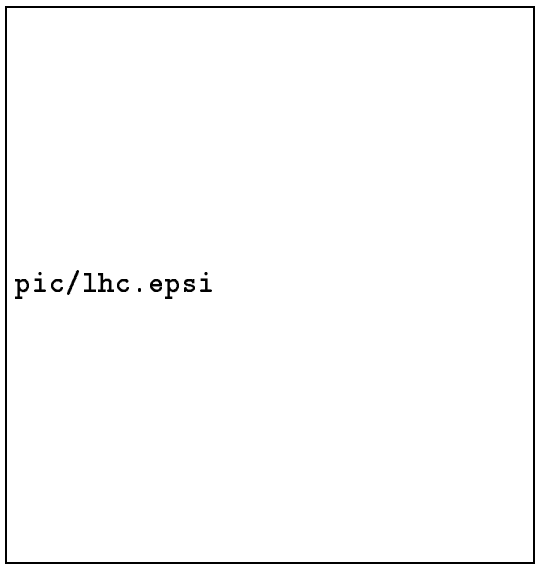

Figure 3.2: The LHC accelerator with the different experiments.

dropping with the energy i.e. the beam is shrunk when it is injected into LHC so it does not take much space.

Two beams will counter-rotate colliding at the experiments with an energy of 7 TeV each. It is the relation

$$p \propto \rho \cdot B$$

where ρ is the bending around the ring and B the magnetic field strength that determines the momenta. To be able to bend with increasing momentum you need to increase the magnetic field strength B, since the radius of the ring is not changed. A field of the order of 9 Tesla can be produced for magnets with the required aperture and with reasonable economic resources. This field is about 100,000 times the earth magnetic field. With this field one will produce an energy of 14 TeV. These high fields put demands on the technique of superconductivity.

LHC proton beam bunches will cross each other forty million times per second. With high luminosity, up to 20 events may occur during each bunch crossing. This give us almost 10^9 events per second containing an enormous amount of data. Acquisition systems are being developed to record data at rates of 10^8 bits per second or more, which is about ten events. This means choosing one event from 10^8 candidates where most of the events will produce uninteresting "splashes" of secondary particles. Sparsely distributed in these

events interesting interactions takes place characterised by some energetic products. To discard the uninteresting events as fast as possible a cascade of decisions will have to be made. These choices are called *triggers* and are very important in the construction of the detector.

3.3 The ATLAS detector

The high energy frontier will be explored by the ATLAS detector in search of the origin of mass and an understanding of the forces of nature. The detector is built up in different layers responsible for detecting different signals. The central part of the detector has as purpose to identify the trajectories of the hundreds of particles created after a proton-proton collision.

The experiment is influenced by the magnetic field configuration. The inner detector superconducting solenoid measures the charged particles momenta before they enter the calorimeter (fig. 3.3). The combination of a toroidal magnetic field in the outer detector with the inner solenoidal field has never been used before. The outer field gives the opportunity to get an independent measurement of the momentum of a particle. With the toroid field one has a strong field even at large rapidities giving a better position measurement.

3.3.1 The Inner detector

There are very hard constraints on the amount of material in the inner detector where damage due to radiation must be considered. Fig. 3.4 shows the structure of the inner detector, where two different technologies are used.

Due to the large track density at LHC you need detectors that can do precision measurements of momentum and vertex [1] position. The solution is semiconductor detectors. In the outer shell the Transition Radiation Tracker gives an identification of the particle and a momentum determination. The detectors cover a region of pseudorapidity $|\eta| \leq 2.5$.

The semiconductor detectors

Semiconductor detectors of Silicon or GaAs (SCT) are used, see fig. 3.4. Semiconductor detectors differs from the gas detectors, they are very compact in size and solid. In the passage of ionising radiation electron-hole pairs are

[1] By vertex one usually means the point where a particle has decayed.

Figure 3.3: The structure of the ATLAS detector with a radius of 11 m and 42 m long.

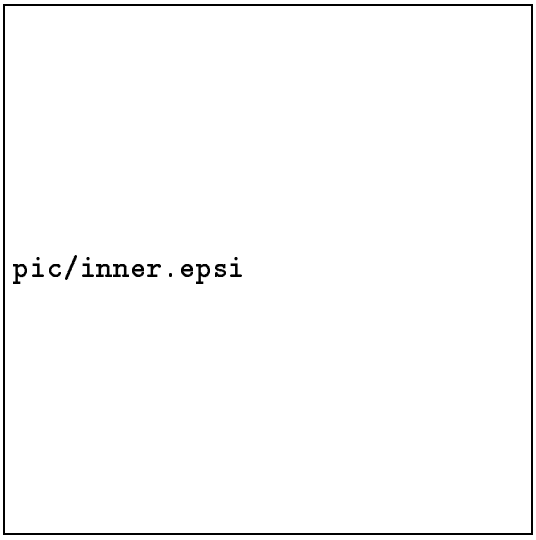

Figure 3.4: The inner part of the detector with the TRT and semiconductor detectors.

created which are separated by an electrical field. The advantage of these detectors are that the average energy required to create an electron-hole pair is much smaller than for gas ionisation. The detector is thus more sensitive and provides a better energy loss resolution. Semiconductor detectors have a greater density giving a higher stopping power than gas detectors. The detectors are important in the reconstruction of secondary vertices due to their good resolution. The problems with these detectors are that they are very expensive and their ability to withstand radiation is not good.

The Transition Radiation Tracker

The outer part of the detector will be filled with the Transition Radiation Tracker. The TRT consists of thin proportional chambers either in the form of straws embedded in fibres or with foils and straws in separate layers. These straws are placed parallel to the beam direction and around 370,000 4mm straws are placed there [5]. Each straw acts as a proportional chamber. When a charged particle crosses the straw ionisation occur and the electrons drift against the anode wire where they are detected, see fig. 3.5. With the help

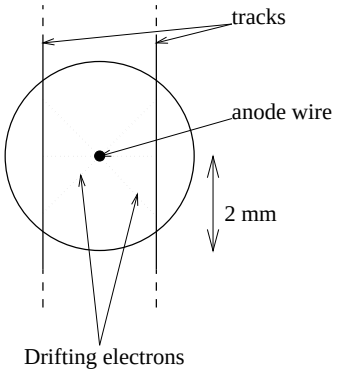

Figure 3.5: In the straw the drift time is a measure of the distance from the anode wire where the track passed. From [5].

from other straws which the particle passed one deals with the ambiguity of on which side the particle passed the wire. This method measures the momentum of the particle track, but gives no identification of the particle. Although the calorimeter provides most of the electron identification the inner detector is useful detecting low energy particles like the electrons from the J/ψ decay. A major problem in the inner detector is that it will be hard to separate electrons from the often produced pions. The solution is to

distinguish between the transition radiation emitted by the different particles that crosses the straw.

The transition radiation is a radiation in the X-ray region which arises when ultra-relativistic [2] particles cross a boundary between two media with different dielectric properties. It increases rapidly with the relativistic γ-factor of the particle defined as

$$\gamma = \frac{E}{mc^2}.$$

Two particles with identical energies but different masses will then emit different amounts of transition radiation. Therefore both identification of the particle and a momentum measurement can be obtained - crucial to distinguish electrons from pions. To create sufficient amount of transition radiation a lot of boundaries are needed. One way to implement this is by using a fibre material where the particles will traverse many dielectric boundaries due to the many individual fibres. The TRT is built up by interchanging layers of fibre to create transition radiation and straws to detect it.

3.3.2 Calorimeters and muon system

The electromagnetic and hadronic calorimeter

The calorimeters are important for measuring the position and energy of a particle. They differ from most other detectors in the way that the nature of the particle is changed by the detector. In contrast to other detectors the calorimeters can detect both charged and neutral particles working as an absorber. During the process the particle will interact with the material generating secondary particles. The calorimeters are often called shower counters since the newly generated particles will interact and a new cascade of particles are created. A signal proportional to the energy of the particle is produced since all the energy of the particle is absorbed in the detector. The absorption process is statistical with a resolution of

$$\frac{\Delta E}{E} \propto E^{-1/2}$$

for the energy measurement [6]. This is of great importance since momentum measurements in a magnetic field for relativistic particles have a resolution proportional to E.

[2] When one talks about the ultra-relativistic region one means a gamma-factor much larger than one.

The electromagnetic calorimeter (fig. 3.3) is a liquid argon calorimeter with lead as absorber placed inside the liquid argon. When a high energy electron or positron interacts with the absorber the dominant energy loss is due to bremsstrahlung, much larger than ionisation losses. For the bremsstrahlung

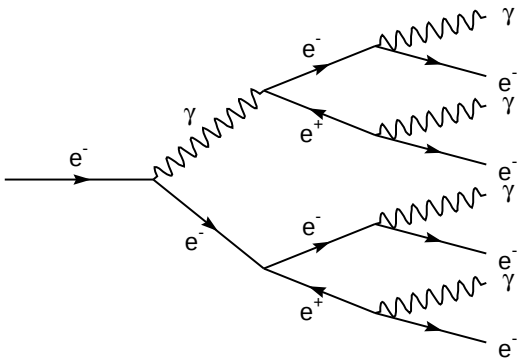

Figure 3.6: Pictorial view of an electromagnetic shower.

photons the dominant absorption process is pair production, leading to a cascade of $e^{\pm}$ pairs. This procedure will continue until the secondary electrons energy loss due to bremsstrahlung is equal to the energy loss because of ionisation. In the ATLAS calorimeter the ionisation is detected with the liquid argon. An electromagnetic shower, as fig. 3.6, will predominantly evolve in the longitudinal direction. It can be easily calculated that the length it travels through the material is proportional to the logarithm of the energy for the incoming particle [6].

The hadronic calorimeter (fig. 3.3) works on the same principle. In the ATLAS detector the thickness of the hadronic calorimeter is crucial. If too many hadrons pass through the calorimeter they can be misidentified as muons in the muon chambers (fig. 3.3).

The muon system

Among the important measurements to be made in the outermost detector layer, the muon spectrometer, is an event with four muons. The four-muon decay is a signal of the Higgs-particle. This requires excellent momentum resolution.

The detection is made inside a toroidal magnetic field. Attached to the toroid are muon chamber planes to measure the muon trajectories. These are placed so a position measurement is possible giving the momenta. The minimum transverse momentum for detecting a muon is around 5 GeV/c, limited by the stopping of low p_{T} muons in the hadron calorimeter.

In the muon system a separate trigger system is developed. When an event takes place the trigger system has to decide whether the information of the event is interesting or not. For the initial running with low luminosity [3] the p_{T} threshold has to be as low as possible. For B-physics a muonic decay of a B-meson is used as level 1 trigger. The present limit is set at p_{T}=6 GeV/c.

3.4 The field of B-physics at ATLAS

The b-quark is the second heaviest constituent of matter, with an effective mass of about 4.5 times that of the proton. The studies in B-physics concerning the heavy b-quark are:

- CP violation. Asymmetry between matter and anti-matter.
- Measuring the mass and lifetime of particles with the b-quark inside.
- Measuring the B oscillation meaning when a B-meson transforms to an anti-B-meson.
- Checking Standard Model predictions of B production and decay rates.

At the beginning of the LHC operation studies in B-physics will take place. This is experimentally easiest with the initial low luminosity $\mathcal{L}$= 10^{33} $\mathrm{cm}^{-2}\mathrm{s}^{-1}$ [1], since pile-up [4] effects are small and vertex detectors very close to the beam pipe are expected to survive for several years.

The ATLAS detector has many properties suitable for B-physics, with a powerful and flexible trigger system. An efficient track reconstruction and electron identification down to low p_{T} is available due to the Transition Radiation Tracker.

The studies of the ($\bar{\mathrm{b}}$c)-system is important because this state is the heaviest one to study, since the t-quark due to its large mass decays before bound

[3] In the beginning of the experiment the luminosity is set to be ten times smaller than the final luminosity. This is referred to as low luminosity.

[4] Meaning several events taking place when the proton bunches interacts.

states can be formed. The study of B_c could give a better understanding of how the strong interaction works.

Chapter 4

How to find the B_C

4.1 Properties of the decay

In the study of B_c the actual particle will not be seen. The B_c decays in a very short time due to its large mass. It is the decay products that can be detected and from them the B_c can be traced. With the decay products we can reconstruct the invariant mass of the B_c. The decay that I have studied to detect the B_c , as illustrated in fig. 4.1 and 4.2, is

$$B_c \rightarrow J/\psi\pi \quad (a) \qquad J/\psi \rightarrow e^+e^- \quad (b) \tag{4.1}$$

with the detectable decay products $e^+e^-\pi$.

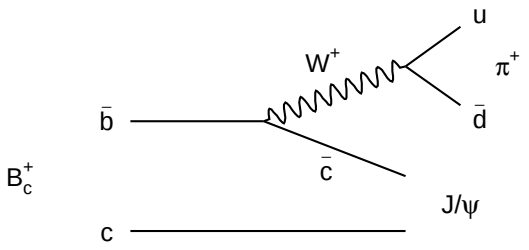

Figure 4.1: The weak decay of the positively charged B_c.

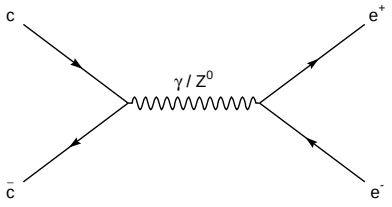

Figure 4.2: The annihilation of the J/ψ decaying into a lepton-pair.

The probability of the decay in reaction 4.1a is small, the branching ratio for $B_c \rightarrow J/\psi\pi$ is calculated to be $0.3 \pm 0.1\%$ [10]. The reason for studying

this decay, though the probability is so small, is that the J/ψ can be mass determined to a high precision. Because there are no neutrinos the decay can be fully reconstructed. The branching ratio for the decay in reaction 4.1b is $6.02 \pm 0.19\%$ [14]. This branching ratio is experimentally measured.

The cross section for the production of b-quarks is dependent on the collision energy. They are created in pairs of $\mathrm{b\bar{b}}$. According to theoretical predictions the total cross section for $\mathrm{b\bar{b}}$-production is taken to be

$$\sigma_{\mathrm{b\bar{b}}} \sim 500 \pm 200 \mu\mathrm{b}$$

at a collision energy of 14 TeV [1]. The probability of a b-quark forming into a $\mathrm{B_c}$ has been calculated by [7] to be in the order of 10^{-3}. From that result one obtain the cross section for $\mathrm{B_c}$-production as

$$\sigma_{\mathrm{B_c}} = \sigma_{\mathrm{b\bar{b}}} \cdot BR(\mathrm{b} \rightarrow \mathrm{B_c}) = 500\mathrm{nb}$$

with cross section

$$\sigma_{decay} = \sigma_{\mathrm{B_c}} \cdot BR(\mathrm{B_c} \rightarrow \mathrm{J}/\psi\pi) \cdot BR(\mathrm{J}/\psi \rightarrow \mathrm{e^+e^-}) = 90\mathrm{pb}$$

for the decay channel.

From the given integrated luminosity $L = 10 f\mathrm{b}^{-1}$ [1] for one year initial running at LHC, the total number of $\mathrm{B_c}$'s produced can be calculated for the decay channel. With the use of eq. 2.3, the total number of $\mathrm{B_c}$'s in the chosen decay channel is

$$N = L \cdot \sigma_{decay} = 900,000$$

integrated over one year. If the uncertainties in the theoretical calculations are implemented the number of $\mathrm{B_c}$ produced per year varies from 300,000 to 2,000,000. Some of these events may be reconstructed.

4.2 The trigger for B-physics

To find some of the 900,000 $\mathrm{B_c}$ occurring in this decay channel, decisions must be made concerning which events that should be saved, since so many collisions takes place. The first trigger the ATLAS detector will look for is a muon with a high transverse momentum (p_{T} >6 GeV/c) and within pseudorapidity range ($|\eta| \leq 2.2$). If this trigger muon is detected it is likely that a b-quark has been produced in the event.

Trigger requirements
LEVEL1 single muon trigger
p_T >6 GeV/c
LEVEL2 single muon trigger
p_T >6 GeV/c
Extra LEVEL2 e^+e^- pair
p_T >1 GeV/c

Table 4.1: The trigger requirements for B-physics. The level 1 trigger is excepted for $|\eta| \leq 2.2$ while the level 2 trigger has an acceptance of $|\eta| \leq 2.5$.

The event will be triggered with a high-p_T muon that mostly comes from the other b-quark not from the B_c. In approximately 10% of all decays the B-hadrons will have a muon in the decay products.

If the first level trigger is passed, the second level muon triggering takes place. At level 2 a sharper p_T-cut is being made on the muon using the precision muon detectors and inner tracking. In [1] extra level 2 requirements are specified. In the event the e^+e^--pair of study must have transverse momenta greater than 1 GeV/c. In the data analysis afterwards extra cuts are applied to discard as many of the uninteresting events as possible. It is important to optimise cuts so that as few uninteresting events as possible goes through.

4.3 Parameters of the track

It is not sufficient to impose cuts on just transverse momenta. It is important also to have parameters that describes the topology of the event.

The impact parameter is a measurement of how far away a particle is from the primary vertex (collision point). The collision point has the coordinates (0,0,0). The impact parameter is defined in the xy-plane since we do not know with high precision where the protons interact along the z-axis ($\sigma_z \approx 5$cm). The precision in the xy-plane is better ($\sigma_x = \sigma_y \approx 15\mu$m), because we know

with good accuracy the position of the beams so they can be tuned in to collide.

If a track in three dimensions is projected on the rϕ-plane (xy-plane) fig. 4.3, then the impact parameter is the shortest distance from origo to the track. If we know the components of the momentum (p_x, p_y) and a position

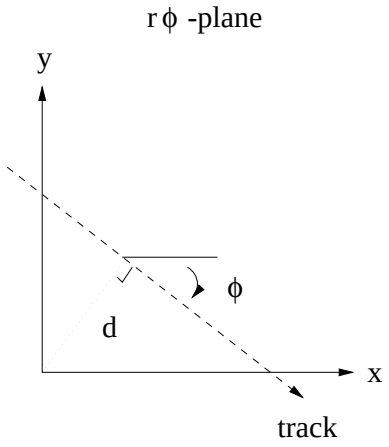

Figure 4.3: The track of the long-lived particles is projected on the xy-plane where the impact parameter, d, is the shortest distance from origo to the track.

of the track (x_t, y_t), the impact parameter d can be calculated. From simple algebra the result is given by

$$d = \frac{p_x \cdot y_t - p_y \cdot x_t}{\sqrt{p_x^2 + p_y^2}} = y_t \cdot \cos\phi - x_t \cdot \sin\phi,$$

as the shortest distance from the primary vertex to the projected track. This distance is coming with a sign. If the projected track is in clockwise direction as in fig. 4.3, the impact parameter is negative. The impact parameter is positive if the projected track direction is counter clockwise.

The angle between the J/ψ and the pion is also a parameter that is of interest in the analysis I performed.

4.3.1 A simple vertex algorithm

The information retrieved by the detector contains information about impact parameter and the angles (d,ϕ,θ). With the knowledge from the simulations it

is possible to calculate the particle tracks in three dimensions represented as a line. For the data analysis from the experiment more sophisticated vertex algorithms are used for calculating the true track which is not a straight line as in my approximation, but a bent trajectory in the xy-plane, since the particles are detected in a magnetic field. The track is parametrised as

$$\vec{r} = \vec{p}t + \vec{r}_0 \tag{4.2}$$

with the momentum as direction vector normalised to one. The vector $\vec{r}_0 = (x_0, y_0, z_0)$ is a point on the line. The aim is to construct the track in three dimensions as a function $\vec{r} = \vec{r}(d, \phi, \theta)$. With the impact parameter and the angle ϕ the coordinates on the track (x_0, y_0) are extracted. After some algebra the result

$$x_0 = -d \cdot \cos\phi \qquad y_0 = d \cdot \sin\phi \tag{4.3}$$

is obtained. The value of z_0 is calculated using the coordinates of eq. 4.3 and the parametrisation of the track.

The squared distance between an arbitrary point $\vec{r_p}$ and the track, $\vec{r}$, is given by

$$D^2 = (\vec{r} - \vec{r_p})^2 = (\vec{p} \cdot t + \vec{r}_0 - \vec{r_p})^2 \tag{4.4}$$

from simple algebra. Minimising eq. 4.4 with respect to the parameter t gives us

$$\frac{\partial D^2}{\partial t} = 0 \quad \Rightarrow \quad t = (\vec{r_p} - \vec{r}_0) \cdot \vec{p}, \tag{4.5}$$

and the value of t is inserted into eq. 4.4. The result is the squared shortest distance between the point and the track

$$D^2_{min} = [(\vec{r}_0 - \vec{r_p}) - [(\vec{r}_0 - \vec{r_p}) \cdot \vec{p}] \cdot \vec{p}]^2 \tag{4.6}$$

with $|\vec{p}|^2 = 1$.

The variables of impact parameter, momentum and angles are parametrised by Gaussian distributions to take into account the detector effects. This will be further discussed in the next chapter. Since the minimised squared distance D^2_{min} is depending on these Gaussian distributed variables, the function of minimisation is depending on three variables - the arbitrary point $(\vec{r_p})$ now denoted as (x, y, z). It is useful to create the function

$$\chi^2(x, y, z) = \sum_{i=1}^{3} \frac{D^2_{min_i}(x, y, z)}{\sigma_i^2} \tag{4.7}$$

with the minimised squared distance and the standard deviations summed over the three tracks. Since the true decay products of the B_c will have the

same vertex point they will obey a χ^2-distribution. This is due to the fact that when the χ^2-function is minimised it will look for the point in 3D-space where the tracks are closest. Indeed this is the vertex point. Therefore the true B_c's will obey a χ^2-distribution with the mean of the degrees of freedom - three [1]. For the false combinations of the B_c's where the tracks can be wherever in space the value of the χ^2-function is arbitrary and does not follow a χ^2-distribution. After the minimisation we know the point that is closest to the three tracks, the true or false vertex point. The decay length in the rϕ-plane [2] is calculated to be

$$L_{xy} = \sqrt{x_v^2 + y_v^2}$$

giving the distance from the primary vertex to the vertex point. It will play an important rôle in the analysis.

[1] The number of degrees of freedom are the number of Gaussian distributed variables minus the number of free parameters in the χ^2-function. In this case there are six Gaussian variables and three free parameters, giving three degrees of freedom.

[2] The reason for evaluating it in this plane is the same as for the impact parameter.

Chapter 5

Simulation and reconstruction

5.1 Event generation

To a priori estimate the expected physics potential of the experiment and to optimise its layout, its performance has to be simulated. The first step in this simulation is to generate proton collisions in a program that uses the known physics laws, the Event Generator.

With the use of the PYTHIA5.7 [2] simulation program collisions of protons of 7 TeV each are simulated. In every of these collisions hundreds of new particles will be created. With the simulation program we can save the interesting events knowing every single particle and its energy, momenta, decay products etc.

For the production of the B_c a b-quark [1] is needed. Simulating general collisions with PYTHIA, approximately one in every hundred event contains a $b\bar{b}$-pair. To save simulation time, the program can be modified so that a $b\bar{b}$-pair [2] is created in every event. Demanding this production means that the $b\bar{b}$-pair is produced in PYTHIA only for lowest order Feynman-diagrams as in fig. 5.1. Doing so the theoretical calculations of the matrix elements in perturbation theory are expanded in a power series of some variable, in this case the strong coupling constant α_s. We could imagine that the corrections are smaller for higher orders (fig. 5.2), but for $b\bar{b}$-production this is not correct. In fact only 10% [3] of the production is due to the lowest order

[1] Since the b-quark is heavier than the c-quark it is much more likely that a B_c is created in an event with a b-quark than in an event with an energetic c-quark transforming into a b-quark.

[2] In the PYTHIA-code this way of generating b-quarks is understood as the MSEL=5 option.

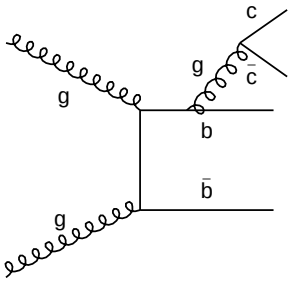

Figure 5.1: Example of lowest order diagrams that produces $b\bar{b}$ and later B_c.

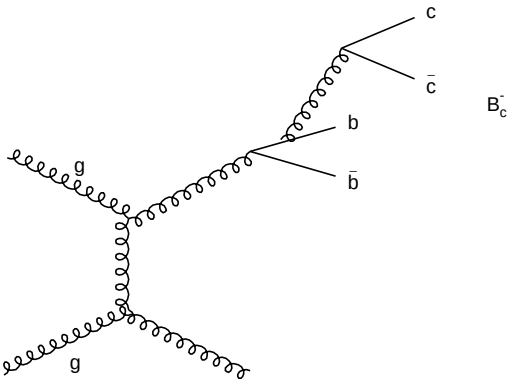

Figure 5.2: A diagram representing higher order corrections to the $b\bar{b}$ cross section.

diagrams as fig. 5.1. This fact could be a problem, but with the results of [4] it is seen that the p_T-spectrum of b-quarks of low p_T has the same shape as for higher order corrections (fig. 5.2) only differing with a constant. Therefore the B_c's produced in diagrams of order α_s^2 (fig. 5.1) are good representatives, looking at the p_T-spectra of the b-quarks.

For the lowest order diagrams the angular topology concerning the creation of b-quarks differ from higher orders. In the lowest order diagrams the b-quarks are usually created back-to-back as in fig. 5.3 with an angle $\alpha \sim \pi$. But for higher order diagrams the angle is smaller (fig. 5.3) because

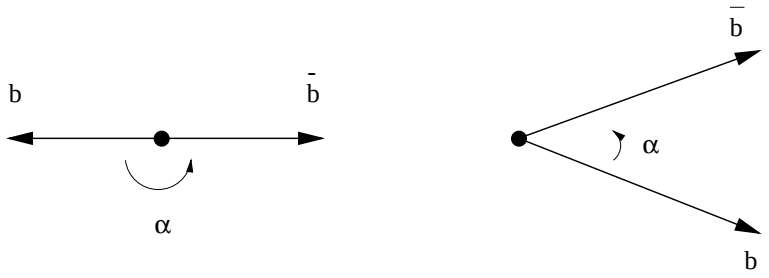

Figure 5.3: The angular topology for the lowest and higher orders of B_c production. For lowest order reactions the b-quarks are emitted back-to-back while in the higher order diagrams the angle is smaller. These drawings are in the centre of mass system.

b-quarks are produced by a gluon splitting into a $b\bar{b}$-pair. In the generation of b-quarks this effect is not taken into account.

The production of c-quarks is not the same as for b-quarks. Instead a b-quark will emit a gluon that splits into a $c\bar{c}$-pair as illustrated in fig. 5.1. This means that there is no easy way to generate the B_c's in every event directly.

Of the B_c's produced only a few percent pass the first trigger level with a muon of p_T >6.0 GeV/c and $|\eta| \leq 2.2$. The program is modified to increase this rate. In the PYTHIA program several variables are defined, one of them the CKIN-parameter. This value sets a lower limit on the p_T for the hard subprocess, that is the process of fig. 5.1 - production of b-quarks. When p_T is increased more energy is inflicted into the system so the cross section of these events becomes smaller. Therefore we try to find a limit of this value so that not so many extra B_c's are produced. The B_c's with the 1st level trigger condition should also be good representatives not differing too much from those that could have been generated without the demand.

A study was made looking at how different p_T-values of this hard subprocess influenced the number of B_c produced with a triggering muon higher than 6 GeV/c within the pseudorapidity range, using the cross sections provided by PYTHIA. The study showed that a value of p_T >8 GeV/c fulfils

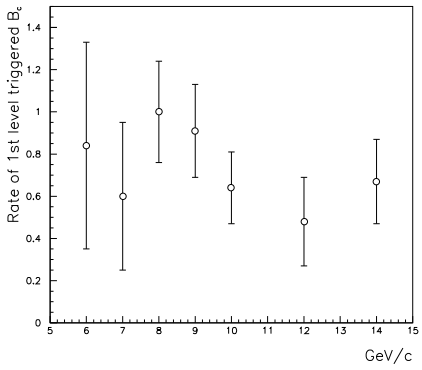

Figure 5.4: The rate of B_c's with a level 1 muon in the event plotted versus the p_T for the hard subprocess in the electron-channel.

the demand that not many extra B_c's are produced. In fig. 5.4 the y-axis represents the rate of production of level 1 triggered B_c mesons normalised to the value of p_T >8 GeV/c. The CKIN-parameter is plotted on the x-axis. The conclusion is that the generated B_c's with p_T^{CKIN} >8 GeV/c and with a triggering muon are as good representatives of B_c's as if they were gen-

erated without the CKIN-parameter. Obviously, more $b\bar{b}$-events should be generated to get the same statistics of B_c's with a triggering muon.

A change was made in the PYTHIA-program to increase statistics of B_c mesons further. The gluon splitting of fig. 5.5 in PYTHIA works in the

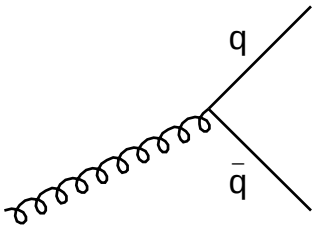

Figure 5.5: The process in fig. 5.1 where the gluon splits into $c\bar{c}$. Generally in PYTHIA, although if it is kinematically possible to create this pair of c-quarks, lighter quarks could be created instead, giving q=u,d,s or c or perhaps b.

following way. Even if the gluon carries the energy needed to create a pair of c-quarks, or more unlikely to create another pair of b-quarks, this does not happen every time. In the program the probability of the quark-creation is the same for the different flavours of quarks lying under the threshold determined by the energy of the gluon. An implementation is performed in the program so that every time it is possible to create a pair of c-quarks it is done. This improves the statistics of B_c's by a factor 4-5, taking into account the production of b-quarks in the split. This gives of course a larger production of c-quarks, because all gluon-splits which have sufficient energy equal to the threshold of the $c\bar{c}$-mass will become $c\bar{c}$-pairs. The other b-quark not creating the B_c could also create c-quarks, but this is not likely to happen since the other b-quark probably has less energy. It could be suspected that this could lead to an increased production of J/ψ, but in the generation only 0.2% more J/ψ's are created, not causing any problems.

5.2 The analysis program

The raw data from PYTHIA are studied with an analysis program. A significant part of the work presented was in the construction of this program. The purpose with the analysis program is to reconstruct the B_c mass from the long-lived particles (electrons and pions) by finding its correct decay products.

In the event generation the signal (B_c) are produced separately from the background of other events. The purpose of the analysis program is to apply it to both the signal and the background and count how many true and false B_c that are reconstructed. To minimise the background and optimise the signal several so called cuts are used. These variables have some characteristics with the signal and one have to know the kinematics of the B_c and background events to choose the right cuts.

The values supplied by PYTHIA are exact but the measurements made in the experiment will not be perfect. With Gaussian distributions one implements the uncertainty of different variables that can be measured with the ATLAS detector. From [1] the parametrisation is given by different resolutions of these variables expressed in standard deviations, σ. The values of PYTHIA are therefore set as mean in a parametrised Gaussian distribution.

- Transverse momenta: $\frac{\sigma_{p_T}}{p_T}$=5.0 $\cdot 10^{-4} p_T \oplus 0.012$
- Angles (θ/ϕ): $\sigma_{\theta/\phi} = 2.0/0.5$ mrad
- Impact parameter (binary pixels): $18 \oplus 61/p_T\sqrt{|\sin\theta|}$ μm
- z-coordinate (binary pixels): $84 \oplus 130/p_T\sqrt{|\sin\theta|}^3$ μm

The notation $A \oplus B$ is equivalent to $\sqrt{A^2 + B^2}$ and p_T is measured in GeV/c. The parametrisation for p_T is set taking into account the initial running with low luminosity where B-physics studies are important.

The electrons and positrons however do not fit this p_T-distribution, they have a worse resolution. The electrons emit bremsstrahlung due to their low mass when they are bent in a magnetic field. This energy loss can be seen by looking at the reconstructed curvature of the particle. An electron that emits bremsstrahlung have higher curvature, giving a false reconstructed momentum because it is proportional to the bending. Bremsstrahlung algorithms have been made reconstructing the momenta of the electron i.e. the path curvature as if the particle had not emitted bremsstrahlung. To include this uncertainty the Gaussian distribution for electrons is given with a worse resolution. According to the results of [1] the reconstruction has been done for electrons of p_T =20 GeV/c giving a resolution depending on the pseudorapidity range. The resolution that was used for $e^{\pm}$ has been extrapolated from these values. For a good resolution of the impact parameter, good vertex detectors are needed for the position measurements.

In the analysis only the electrons, positrons and pions are of interest. Since the ATLAS detector cannot see the difference between pions and

charged K-mesons, they are also treated as pions. In every event all electrons and positrons are reconstructed and their tracks are determined. This is done in the simulation as well as in the experiment (although in a different way). The demand is that the track lies in the detector coverage i.e. $|\eta| \leq 2.5$ and that it survives the cut on p_{T}. All combinations of $\mathrm{e}^+\mathrm{e}^-$ are made up calculating the invariant mass of the pair. If the mass is close to the J/ψ-mass one has a J/ψ candidate. All these are combined with pions calculating the invariant mass, giving a true or false $\mathrm{B_c}$. For the $\mathrm{B_c}$-candidate there are some restrictions: The tracks of the three particles are fitted giving a χ^2-value of how good the fit is (see fig. 5.6). The χ^2-function, defined in eq. 4.7, is calculated as

$$\chi^2(x,y,z) = \sum_{tracks} \left(\frac{d_{xy}^2}{\sigma_{ip}^2} + \frac{d_z^2}{\sigma_z^2} \right)$$

in the program. The function is divided into two parts because the resolutions that affect them are not the same. From the fit information is gained about

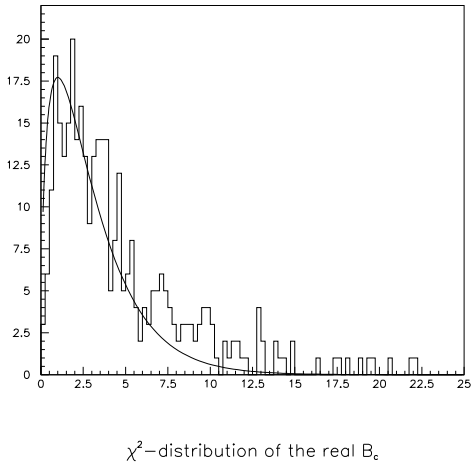

Figure 5.6: The χ^2-distribution of the $\mathrm{B_c}$ compared to the χ^2-function (smooth curve) with three degrees of freedom.

the reconstructed secondary vertex of the electrons and pion, and a cut is made on the decay length from primary vertex. A cut is also made on $\cos\beta$, where β is the angle between the pion and the J/ψ.

Chapter 6

Results

6.1 Introduction

The mass of the B_c and its excited state B_c^* were set to be 6.258 and 6.320 GeV/c^2 according to [11]. The lifetime of B_c was set to be 1 ps. The masses of the c- and b-quarks were defined as 1.3 and 4.5 GeV/c^2. A total of 13,912

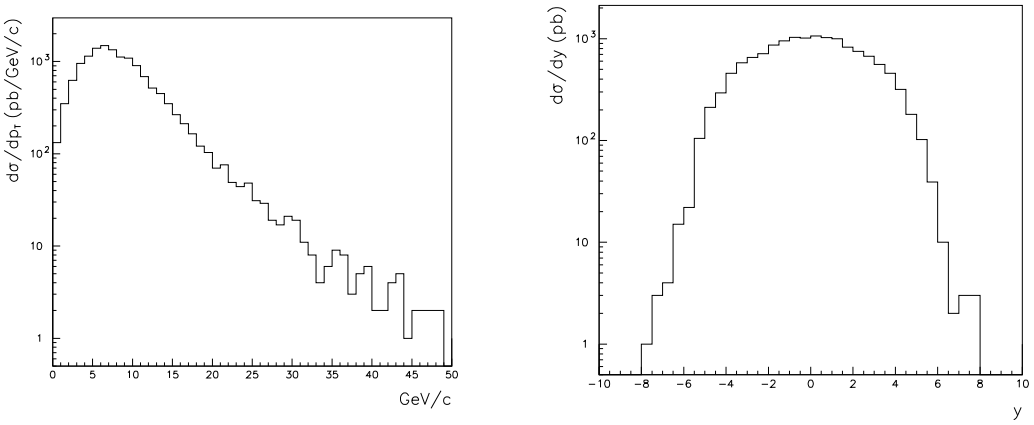

Figure 6.1: The distributions of p_T and rapidity for generated B_c-mesons normalised to $\sigma_{B_c} = 500$ nb.

B_c-mesons were generated with the simulation technique as described in the previous chapter. This corresponds to approximately 28 millions of generated $b\bar{b}$-events, taking a lot of computer time. In fig. 6.1 the p_T- and rapidity-distributions for the B_c are shown, normalised to a cross section of 500 nb.

The shape of the distributions look like the theoretical predictions of [12] [1] but the distributions are not true for a general B_c due to simulation with the CKIN-parameter. Only the B_c with high p_T should follow the p_T-distribution.

6.2 The B_c-signal analysis

With an assumed cross section of 500 μb for beauty production at LHC a total of $5 \cdot 10^{12}$ pairs of $b\bar{b}$ are produced per year, given an integrated luminosity of 10 fb^{-1} [1]. Since the B_c generated with the CKIN-parameter are good representatives only if the event contains the 1st level trigger, it is important to know how often this occur. According to the Technical Proposal [1] suggested for the ATLAS experiment around 0.46% of the $b\bar{b}$-events have this first trigger. The cross section for the process to occur is

$$\sigma_{b\bar{b},muontrig} = 0.46\% \cdot \sigma_{b\bar{b}} = 2.3 \pm 0.9 \mu b$$

with the $b\bar{b}$ cross section from Chapter 4. In the analysis 974 B_c fulfilled this demand.

Shown in tab. 6.1 are the different cuts that are applied after the 1st level muon trigger. The cuts are implemented in the same order as tab. 6.1 and

Geometry	Acceptance
$\|\eta\|_e \leq 2.5$	73%
$\|\eta\|_\pi \leq 2.5$	94%
2nd level trigger	Acceptance
$p_T(e) > 1$ GeV/c	74%
$p_T(\pi) > 1$ GeV/c	91%
Reconstruction	Efficiency
$\Delta M(J/\psi) < 50$ MeV	86%
$\cos\beta > 0.25$	90%
$\chi^2 < 8$	83%
$L_{xy} > 300$ μm	57%
Track reconstruction	90%
TOTAL	15%

Table 6.1: The number of true B_c that pass each cut. With 974 B_c with 1st level trigger, around 150 are left after the cuts.

[1] The normalisation of the distribution is not the same as for [12].

the percentage shows how many B_c that are left when the cuts are applied one after another. The cuts on pseudorapidity are defined from the range of the detector. The demand on the p_T of the electron clearly fulfil the condition set for the extra level 2 requirements of [1]. The cut on the angle between the J/ψ and the pion is very efficient for the combinatorial background of the event. In fig. 6.2 the cos β-statistics are shown for B_c and combinatorial

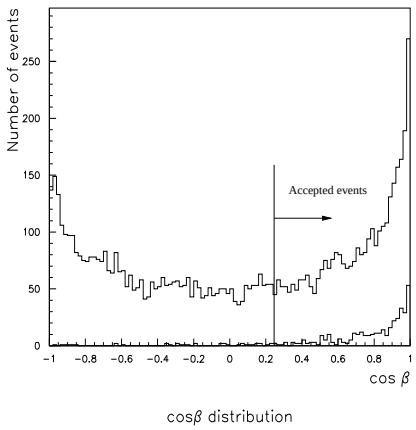

Figure 6.2: The cos β-statistics for signal (lower distribution) and combinatorial background (higher distribution).

background.

The combinations that pass these cuts are shown in fig. 6.3. The mass distribution of the B_c is displayed with the combinatorial background. The combinatorial background has no elements near the mass region of the B_c-peak. The area of the B_c-signal is fitted with a Gaussian distribution. It should follow such a distribution since the variables it depends on does. The mean value from this fit is 6.260 GeV/c^2 in good agreement with the value of 6.258 set in PYTHIA, and a resolution from the fit of about 52 MeV/c^2. The number of B_c produced during one year of running [2] is calculated to be

$$N_{B_c} = L \cdot \sigma_{b\bar{b},muontrig} \cdot BR(b \rightarrow B_c \rightarrow J/\psi\pi) \cdot BR(J/\psi \rightarrow e^+e^-) \cdot \varepsilon_{rec} \quad (6.1)$$

with the values of Chapter 4.1. It is standard to look at a mass window of 2.8 standard deviations in the distribution. That is in the region

$$m_{B_c} \pm 1.4\sigma = 6.260 \pm 0.074,$$

[2] Meaning 1/3 of a year $\sim 10^7$ s.

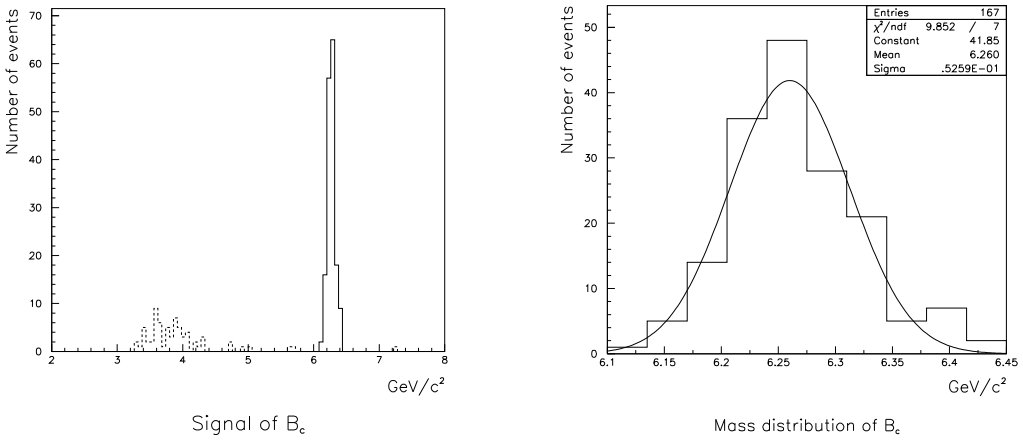

Figure 6.3: The left figure shows the mass distribution of the B_c with a clear peak. The hatched distribution represents the combinatorial background from the B_c-events. In the right figure a Gaussian fit is made to the distribution of real B_c's.

one counts the number of B_c's. This region corresponds to a mass window between 6.186 - 6.334 GeV/c^2 with 139 B_c, that gives us a reconstruction efficiency of 13% within the mass window. With the given parameters eq. 6.1 is evaluated with a statistical error giving the result

$$534 \pm 45(stat)$$

reconstructed B_c per year. The statistical interpretation that random drawn B_c's from the mass window region also are normally distributed gives us

$$\sigma_{B_c} = \frac{\sigma_{peak}}{\sqrt{N_{B_c}}} \approx 4.5 \quad \mathrm{MeV}/c^2$$

for the mass determination of B_c.

If we invoke the large uncertainties of the $b\bar{b}$ cross section and branching ratios for B_c-production and the decay to $J/\psi\pi$, the number varies from 150-1100 produced B_c per year.

6.3 The background analysis

The background that fakes B_c events clearly comes from $b\bar{b}$-events. The production of J/ψ in the primary vertex ($c\bar{c}$) is not taken into account since

it is unlikely to have a high p_T muon in the event. In the production of b-quarks two possible backgrounds are concerned:

- B-mesons decaying into a J/ψ. This gives us a J/ψ in a secondary vertex, which a vertex fit does not take away. It could then combine with a high energetic pion faking a B_c.
- Electrons and positrons coming from leptonic or semi-leptonic decays could fake a J/ψ and combine with a pion.

In the generation of background the same CKIN-parameter was used as for the signal and only lower order diagrams were generated. The J/ψ was also forced to decay to e^+e^- to study the effect of real J/ψ's from B-mesons. To increase statistics it was implemented that all the anti-B-mesons were to decay to a muon and anything. It was observed that "anything" predominantly was different kinds of D-mesons, always decaying together with the muon. These D-mesons are very dangerous since they often decay to electrons which will be in a secondary vertex.

The background was analysed in parallel with the signal. The cuts of tab. 6.2 are very efficient in suppressing the background, leaving most of the signal. The effect these cuts have on the background are compared with the

Reconstruction	Signal	Background
$\Delta M(J/\psi) < 50$ MeV	86%	22%
$\cos\beta > 0.25$	90%	44%
$\chi^2 < 8$	83%	31%
$L_{xy} > 300$ μm	57%	33%
TOTAL	37%	1%

Table 6.2: The reconstruction efficiencies of the signal compared with the background. The cuts are applied one after another.

signal. It seems that the knowledge of the good mass determination of J/ψ is extremely efficient.

The background collected after these cuts contained of 848 fake B_c. One should not compare these plots with the one of the signal because the integrated luminosity is not the same. One should also remember that the background from real J/ψ is favoured by a factor 20, since it has been forced to decay into e^+e^-. In the decay mode

$$B \rightarrow J/\psi X$$

most of the time X is a pion/kaon or several pions. In the background signal we should then see the real J/ψ combine with a correct pion in many cases. This means that the invariant mass of this system cannot be larger than the

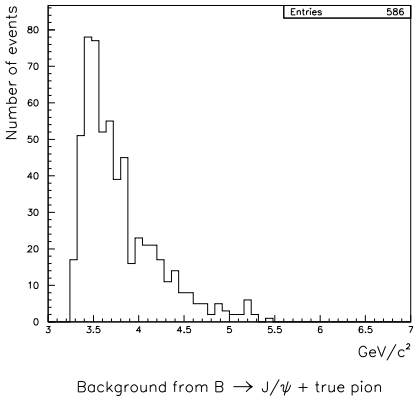

Figure 6.4: The true J/ψ from a B-decay has combined with a pion from the same decay. In case of a several pion-decay the invariant mass is of course lower, but always less than 5.5 GeV/c^2.

masses of the B-mesons ($B^{\pm}, B^0, B_s^0$), that is less than 5.5 GeV/c^2. In fig. 6.4 the background from these events are plotted. It clearly shows that this background can be neglected since the mass distribution will not interfere with that of the B_c.

The remaining 261 background events are split up in two plots (fig. 6.5). One representing the real J/ψ combining with a pion that does not come from the same vertex, and one of fake reconstructed J/ψ. The statistics of fig. 6.5 is not impressing, but this is always a problem in simulating rare events. If we impose smart cuts we could remove all the background coming from leptonic decays, but with the poor statistics this would not be right, some events will be reconstructed. In the background from the leptonic decays an electron from a D-meson or π^0 (the π^0 coming from an excited D-meson decaying into $e^+e^-\gamma$) combine with a positron from the other side coming from a B- or D-meson. With a sophisticated secondary vertex algorithm it should be possible to suppress these decays.

An estimate of the background produced in one year can be achieved by the following method. Assuming a nearby flat background in the range of 5.5 - 7.0 GeV/c^2 of fig. 6.5, the mass distribution (number of background events

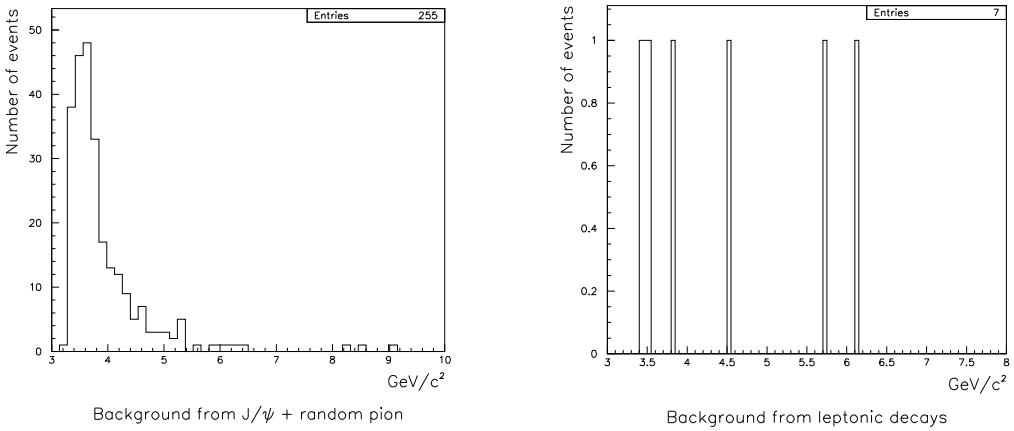

Figure 6.5: The left figure shows the background from true J/ψ's combined with a random pion/kaon not from the decay. On the right the background from fake J/ψ's. The background on the left figure is favoured since the J/ψ is forced to decay to electrons.

per GeV/c^2) is calculated. Counting the events in the mass region the result

$$\frac{6 \cdot 0.06 + 2}{1.5} = 1.57 \quad \text{events/GeV}/c^2$$

is obtained. The number of events (6 and 2) in this mass region can be seen in fig. 6.5, with the six events from real J/ψ events normalised since it was forced to decay into e^+e^-.

The number of background events produced in one year can be calculated according to the formula

$$N_{fake} = L \cdot \sigma_{b\bar{b},muontrig} \cdot \varepsilon_{fake}$$

with the reconstruction efficiency ε_{fake} of the fake B_c's. Looking at the same mass window as the signal i.e. 145 MeV/c^2, one can calculate the number of background events to be 0.23 within 145 MeV/c^2. The number of generated events that fulfils the 1st level muon trigger is around 270,000. Taking into account the track reconstruction efficiency of 90% a fake reconstruction efficiency of

$$\varepsilon_{fake} = 7.7 \cdot 10^{-7}$$

is obtained. The results leads us to a total of $\sim$ 18,000 background events per year. The analysis shows that the dominant background comes from the leptonic decays faking a J/ψ.

In fig. 6.6 the mass spectrum is plotted for background and signal. It could look like this in the results from the experiment. The background is fluctuating around 18,000 and on top of it one sees a little peak. To test

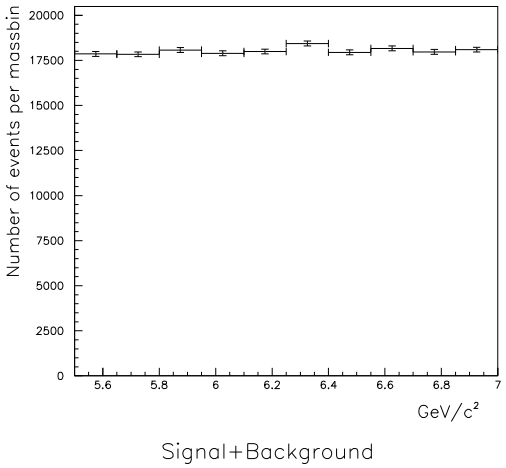

Figure 6.6: An impression of how the B_c-signal in the electron channel could look like after 1 year of running at LHC.

whether the seen peak really is a peak and not statistical fluctuations the statistical significance of the peak is calculated. It is defined as

$$S = \frac{signal}{\sqrt{background}},$$

and in particle physics it is believed that if the significance is greater than five, then it is observable. In the analysis with a signal of $\sim$ 500 and a background of $\sim$ 18,000, a statistical significance of 4 is calculated. These figures correspond to one year of data taking. In the experiment data will be taken for three years improving the statistics by a factor three. This is of course enhancing the significance with a factor $\sqrt{3}$, giving the value 7.

6.4 Conclusions

In the study of the decay channel $B_c \rightarrow J/\psi\pi$ with $J/\psi \rightarrow e^+e^-$ a total of $\sim$ 500 B_c can be reconstructed after one year. Taking into account the error of the theoretical calculations, which is much larger than the statistical

error, a total of 150 - 1100 B_c are produced per year. The mass of the B_c can be measured with a resolution of ~ 4.5 MeV/c^2. The background events are estimated to be in the order of 18,000 events per year giving a statistical significance of 4. After three years of data taking a significance of 7 is achieved. If the theoretical predictions of cross sections and branching ratios are in good agreement with the experimental values, and with a reasonable background, then the B_c will be visible in the decay channel.

6.5 Outlook

It is hard to criticise ones own work, but I will try to discuss some of the uncertainties and assumptions that are made.

- In the generation of signal and background only lowest order diagrams are generated. Although there is an argument that the p_T-distribution has the same shape for lowest and higher orders, the angular correlations of b-quark production is not the same. The angular correlation could be important for the background since decaying leptons from produced B-mesons or later D-mesons get tracks closer together. They could more easily reconstruct a fake secondary vertex.

- The ATLAS sub detectors have to be very good. The misidentification of hadrons could give a large contribution to the background. A hadron, e.g. a pion, could be misidentified as an electron and then combine with an electron to form a fake J/ψ. This background is ignored in the present analysis.

- In the theoretical calculations of the lifetime of the B_c, there are some contradictions. According to [11] a lifetime of 1 ps could be expected, but in the calculations by [13] they predict a lifetime between 0.4-0.7 ps. If the decay time was smaller the result would be worse because the density of other tracks increases when the decay length for the B_c becomes smaller. The uncertainties according the probability of creating a B_c is large, one only knows to order what it could be.

Acknowledgement

I would like to thank Ulrik Egede for his efforts in answering my millions of questions and for showing interest in my work. Many thanks also to Jenny Ivarsson and Torsten Åkesson for making this thesis possible. I would also like to thank Miguel Sanchis-Lozano and Torbjörn Sjöstrand for valuable discussions.

Appendix A

The invariant mass

In physics we want all physical laws to be the same for all observers in different Lorentz-systems. With the knowledge that a tensor-equation is valid in all coordinate-system, we can rewrite all physical laws as a tensor equation. In special relativity, where four-vectors with coordinates and time are used, the coordinates can be written as $x^\mu = (ct, \vec{r})$, μ running from zero to three. The dot-product is an invariant entity i.e. it is valid in all inertial systems. In tensor algebra the dot-product is defined as

$$x^\mu \cdot x_\mu$$

or with the use of the metric tensor $g_{\mu\nu}$ as

$$x^\mu \cdot g_{\mu\nu} x^\nu$$

This can be applied to the four-momenta describing the kinematical state of the particle, $\vec{P} = (E, \vec{p})$ [1]. Consider a system of N particles each described by their four-momentum P^μ. The invariant mass (W) of this system can be written as

$$W^2 = \sum P_i^\mu \cdot \sum g_{\mu\nu} P_j^\nu = \sum P_i^\mu \cdot \sum P_{j\mu}. \qquad \text{(A.1)}$$

The metric tensor $g_{\mu\nu}$ can be written as a matrix

$$g_{\mu\nu} = \begin{pmatrix} 1 & 0 & 0 & 0 \\ 0 & -1 & 0 & 0 \\ 0 & 0 & -1 & 0 \\ 0 & 0 & 0 & -1 \end{pmatrix}$$

[1] Natural units i.e c=1

and from this one obtain the result

$$g_{\mu\nu}P_i^{\nu} = P_{\mu} = (E, -\vec{p})$$

Evaluating equation A.1 gives us the relation

$$W^2 = (E_1 + \ldots + E_N, \vec{p}_1 + \ldots + \vec{p}_N) \cdot (E_1 + \ldots + E_N, -\vec{p}_1 - \ldots - \vec{p}_N) = E_{tot}^2 - p_{tot}^2,$$

the invariant mass of a system of N particles. In dealing only with one particle, the four-momenta in the rest frame is given by $P^{\mu} = (m, 0)$. Since the dot product of this four-momenta is the same in all inertial systems we get

$$m^2 = E^2 - p^2,$$

which is a well known result in special relativity.

Bibliography

[1] The ATLAS collaboration. ATLAS technical proposal. Technical Report CERN/LHCC/94-43, CERN, December 1994.

[2] H.-U. Bengtsson, T. Sjöstrand. Computer Physics Commun. **46** (1987) **43**

[3] CERN, Theory division. PYTHIA 5.6 and JETSET 7.3 Physics and manual, CERN-TH.6488/92 edition, September 1992.

[4] J.R. Cudell, O. Di Rosa, I. ten Have, A. Nisati, R. Odorico, T. Sjöstrand. A Comparison of Bottom Production in Different Event Generators, Large Hadron Collider Workshop , Aachen (1990).

[5] U. Egede. Electron Identification with the ATLAS Detector at the Large Hadron Collider. LUNFD6/(NFFL-7121) 1996.

[6] B.R. Martin, G. Shaw. Particle Physics. John Wiley & Sons, 1994.

[7] E. Braaten, K.Cheung, T.C. Yuan. Phys. Rev. **D48** (1993) 5049.

[8] A.V. Berezhnoy, A.K. Likhoded, A.V. Tkabladze. Hadronic production of B_c-mesons. **IHEP 94-48** .
S.S. Gershtein, V.V. Kiselev, A.K. Likhoded, A.V. Tkabladze. Physics of B_c-mesons. **IHEP 94-81** .

[9] M. Galdon, R. Perez Ochoa, M.A. Sanchis-Lozano, J.A. Walls. Searching for B_c mesons in the ATLAS experiment at LHC. IFIC/95-62 (hep-ph/9510450).

[10] A. Leike, R. Rückl. Nucl. Phys. **B** (Proc. Suppl.) **37B** (1994) 215.

[11] E.J Eichten, C. Quigg. Mesons with beauty and charm: Spectroscopy. FERMILAB-PUB-94/032-T.

[12] K. Kolodziej, A. Leike, R. Rückl. Production of B_c Mesons in Hadronic Collisions. Phys. Lett **B355** 337-344 (1995).

[13] M. Beneke, G. Buchalla. The B_c Meson lifetime. Phys. Rev. **D53** 4991-5000 (1996).

[14] R.M Barnett et al. Particle Data Group. Phys. Rev. **D54** (1996).